Chemical Engineering Journal 529 (2026) 173295

Contents lists available at ScienceDirect

Chemical Engineering Journal

journal homepage: www.elsevier.com/locate/cej

Short Communication

The art of evasion at the nanoscale: Engineered CuS nanovaccines resist extracellular sequestration in plants

Yash Boyjoo [a], Junseo Lee [b], Chu-Yun Hwang [b], Luyao Qin [c], Yi Wang [c], Jason C. White [c], Qian Chen [b], Archana Bhaw-Luximon [a,*]

[a] Biomaterials, Drug Delivery and Nanotechnology Unit, Centre for Biomedical and Biomaterials Research, University of Mauritius, Reduit, 80837, Mauritius
[b] Department of Materials Science and Engineering, the Grainger College of Engineering, University of Illinois, Urbana, IL, 61801, United States
[c] The Connecticut Agricultural Experiment Station (CAES), 123 Huntington Street, New Haven, CT, 06511, United States

ARTICLE INFO

Keywords:
Particle tracking
Nanoparticle engineering
Nanoparticle–plant interactions

ABSTRACT

Plant nanovaccines, particularly copper-based nanomaterials, have emerged as promising alternatives to conventional pesticides and fungicides in agriculture. While being sustainable and effective in mitigating biotic and abiotic stresses, their mechanisms of action in plant systems remain unclear due to the complexity of plant responses. Here, advanced imaging techniques including X-ray micro-computed tomography, scanning and transmission electron microscopy, and elemental mapping were employed to track the defence responses to copper sulfide (CuS) particles inside the leaves of *Fusarium oxysporum f. sp. Lycopersici* (a fungus that causes vascular wilt disease) infected tomato plants. The preliminary results suggest that commercial bulk CuS microparticles (bCuS) triggered sequestration by endogenous calcium oxalate crystals, resulting in isolation from plant cells (potentially uncovering a previously unrecognized plant defence mechanism against foreign particles). Conversely, nanoengineered iron (Fe)-doped CuS nanoparticles (nFeCuS), owing to their nanosize, morphology, and surface properties, evaded this defence mechanism and remained bioavailable within mesophyll tissues. These findings underscore the value of advanced imaging tools for resolving particle–plant interactions at the nanoscale-level and lay the groundwork for the design and engineering of next-generation nanovaccines tailored to specific crops and stress conditions.

1. Introduction

A new paradigm shift in agriculture is emerging, centered on the One Health concept, which emphasizes the interconnectedness of human, animal and environmental health. Among many technologies, nanoplatforms with proven success in human health are currently under extensive evaluation in agriculture for their potential as tools that respond to specific biotic and abiotic plant stresses. For example, the mechanisms of action of nanoscale drugs delivery systems in humans are well-studied by evidence-based clinical studies, which have facilitated transition from laboratory research to bedside applications for complex diseases such as cancer [1] as well as for nanovaccine technologies exemplified by recent commercial mRNA vaccines [2] for immunization and ongoing efforts to develop similar treatments for lethal cancers [3]. These nanodelivery systems have proven capacities to precisely deliver poorly soluble molecules, achieve transcellular transport and distribute multiple drugs to targeted site of action for specific cells.

To enhance climate resilience and ensure global food security and safety, there is an imminent need to adapt the nanoplatforms established in human healthcare for agriculture, to transform efficient agrochemical delivery through the use of nanofertilizers and nanovaccines, with plants serving as the new model for applications. Nanovaccines can enhance plant defence against abiotic and biotic stresses by acting as elicitors that generate reactive oxygen species (ROS) and activate defence signalling pathways [4,5], thereby improving targeting precision, reducing chemical inputs, and minimizing environmental contamination and resistance development compared to conventional pesticides. However, there remains limited understanding of the mechanisms of action of nanovaccines in plants. Plants responses to nanovaccines are phenomenologically dependent on the nanomaterial type, environment, exposure dose, timing, and the plant species [6,7]. Foliar-applied nanovaccines can enter leaves through the stomata and cuticle [8] but an understanding of their physiological interactions within leaf tissues as first point of entry, especially on the nano to

* Corresponding author.
E-mail address: a.luximon@uom.ac.mu (A. Bhaw-Luximon).

https://doi.org/10.1016/j.cej.2026.173295
Received 22 November 2025; Received in revised form 15 January 2026; Accepted 20 January 2026
Available online 21 January 2026

microscale, remains unexplored [9–12].

Copper-based nanoparticles (NPs) have attracted increasing interest since the early 2010s as next-generation substitutes for traditional pesticides and fungicides, offering both antimicrobial efficacy and reduced environmental impact [13–16]. Herein, we image and characterise the temporal mechanism of interactions between foliar-applied model copper-based plant nanovaccines including commercial bulk-CuS (bCuS) microparticles (MPs) and nanoengineered iron-doped, citrate coated CuS NPs (nFeCuS, see methods in the Supplementary information, SI) and *Fusarium oxysporum f. sp. Lycopersici* infected tomato plants. CuS was selected because it exhibits distinct physicochemical properties, including tunable dissolution kinetics, and has demonstrated superior disease-suppressing performance compared with other Cu-based materials [15]. In addition, sulphur (S) can have synergetic effects with Cu [17,18] and as an essential macronutrient, may provide supplementary nutritional benefits to the plant. Tomato leaves contain endogenous prismatic calcium oxalate (CaO_x) crystals which can sequester adsorbed toxic metal ions [19–21], although interactions with particles currently remain unknown. Here, we studied the interaction between the particles and the plant's defence system using a suite of imaging tools across length scales, including X-ray tomography, scanning electron microscopy (SEM), scanning transmission electron microscopy (STEM) and energy dispersive X-ray spectroscopy (EDX), Fig. 1a. X-ray tomography enabled 3D visualization of CuS particle dynamics within tomato leaf tissues at ~370 nm resolution, supported by electron microscopy and elemental mapping. Preliminary results suggest that bCuS MPs triggered a sequential defence response involving sequestration by endogenous CaO_x crystals, followed by agglomeration and isolation from plant cells. Conversely, nFeCuS NPs, owing to smaller size, distinct morphology, and surface properties, evaded this mechanism and remained bioavailable within mesophyll tissues. These findings unveil a fundamental mechanistic distinction in how particle nanoengineering dictates plant defence evasion and intracellular bioavailability.

2. Results and discussion

We recently reported on the impact of different types of CuS NPs on enzymatic activity, disease progression and the genetic profile of *Fusarium* infected tomato plants as compared to bCuS and $CuSO_4$ [22]. CuS NPs, particularly nFeCuS enhanced the disease resistance of tomato plants by boosting the activity of ROS-scavenging enzymes and modulating key defence-regulated genes.

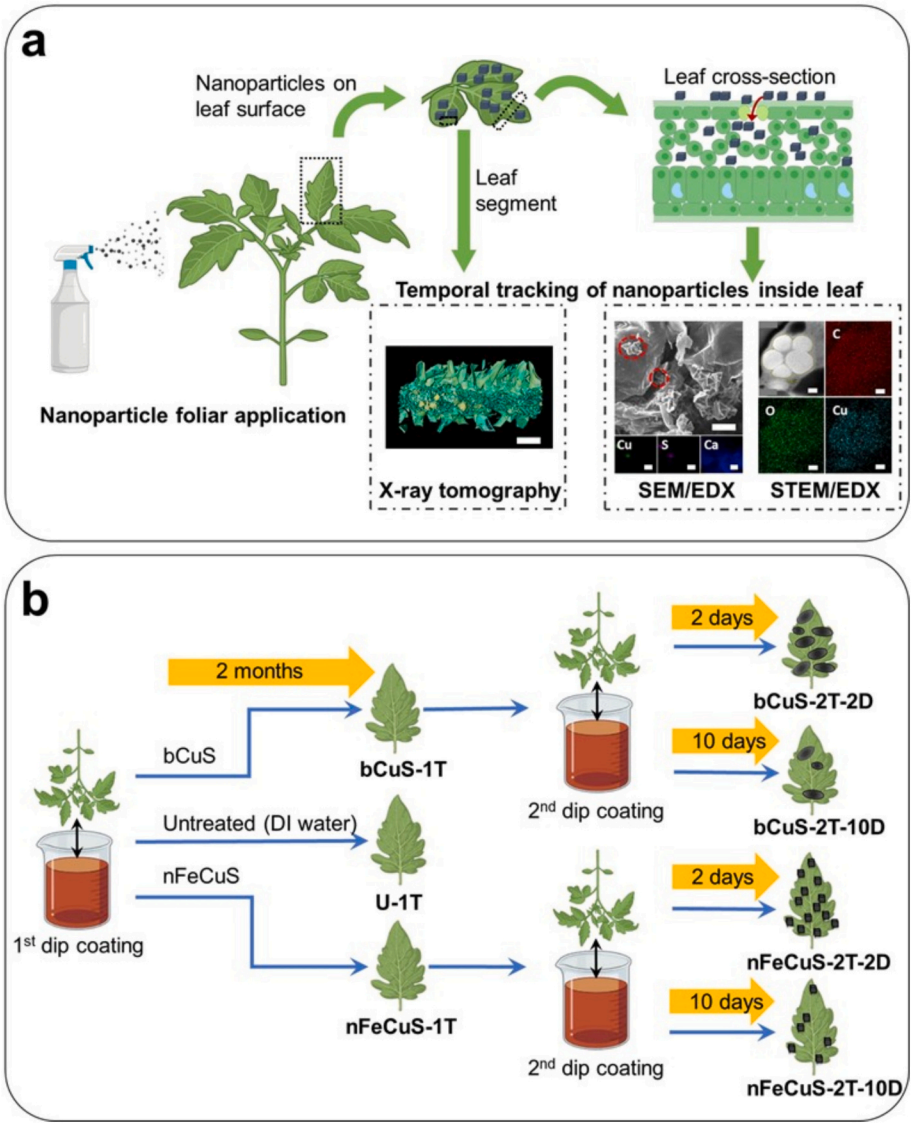

Fig. 1. a) Orthogonal strategies to track the temporal physiological interaction of CuS nano- and MPs in tomato leaves. b) Schematic of the dip-coating protocol of *Fusarium* infected tomato plants in 200 mg L^{-1} CuS particles suspension and the different leaf samples taken for characterization.

In the current study, three-weeks-old *Fusarium*-infected tomato seedlings were dip-coated in a 200 mg L^{-1} particle suspension of either bCuS or nFeCuS, while deionized (DI) water was used for the untreated control. Cu-based NPs have previously been applied to crops such as soybean (*Glycine* max), watermelon (*Citrullus lanatus*), and tomato (*Solanum lycopersicum* L.) across a broad concentration range (10–1000 mg L^{-1}) [23–26]. In the present study, a moderate nano/microparticle suspension concentration of 200 mg L^{-1} was employed. This concentration was selected based on our earlier findings showing improved resistance of tomato plants to *Fusarium* infection [22]. After two months, leaves were sampled from the plants and designated as U-1T (untreated), bCuS-1T, and nFeCuS-1T, where "1 T" indicates the first treatment (Fig. 1b). The two-month interval was considered adequate to allow near-complete dissolution and translocation of the particles within the plant, thereby serving as an appropriate reference for comparison with leaf samples collected at shorter post-treatment intervals. Immediately following this initial sampling, a second dip-coating treatment was administered to the particles-treated plants. Leaf samples were then collected 2 and 10 days after this second treatment and designated as bCuS-2T-2D and bCuS-2T-10D for the bCuS-treated plants, and nFeCuS-2T-2D and nFeCuS-2T-10D for the nFeCuS-treated plants. Here, "2T" denotes the second treatment, and "2D" and "10D" indicate the number of days post-treatment. The leaf samples were subsequently analysed using a combination of X-ray tomography, SEM, STEM, and EDX.

2.1. Imaging of untreated and CuS treated tomato leaves

X-ray absorption is proportional to material density and atomic number. To visualize the dense, high atomic number particles embedded within the leaf tissue, image processing was necessary (see methods in

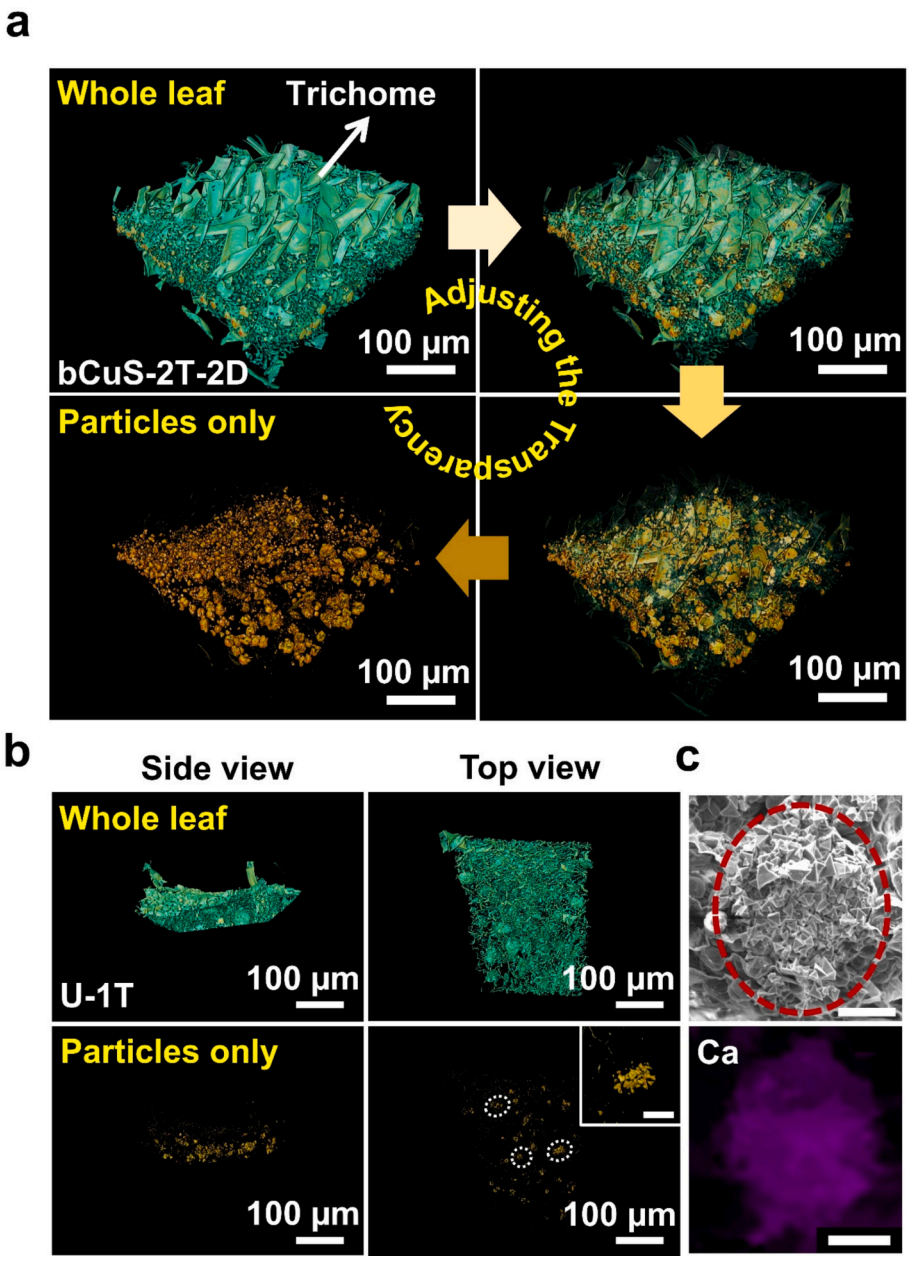

Fig. 2. a) 3D rendering of X-ray tomography images obtained with sample bCuS-2T-2D. The steps in adjusting the transparency are shown to divulge particles inside the leaf. b) Side and top X-ray tomography images of sample U-1T showing whole leaf (top) and particles only (bottom). Inset in the particles only top view shows a cluster of CaO_x crystals inside an idioblast. The scale bar is 20 µm. c) SEM image and EDX mapping for Ca of CaO_x crystals inside an idioblast cell in sample U-1T. The scale bar is 10 µm.

SI). Fig. 2a displays the sequential transparency adjustments used to isolate and visualize solid particles, using sample bCuS-2T-2D as an example. Trichomes, which are hair-like epidermal structures composed primarily of low atomic number elements such as carbon (C), oxygen (O), and nitrogen (N), were used as reference points. By tuning the image transparency until the trichomes faded from view, only high-density particles composed of heavier elements such as Ca and Cu remained visible. Fig. 2b presents the side and top views of X-ray tomography images for sample U-1 T, showing both the whole leaf structure and the isolated solid particles. Interestingly, solid particles were observed within the untreated leaf tissue that were attributed to endogenously formed prismatic CaO_x MPs, typically localized within idioblast cells of tomato leaves (the inset in Fig. 2b shows a cluster of CaO_x particles) [20]. This interpretation is supported by complementary SEM and EDX analyses (Fig. 2c) which confirmed morphology and elemental composition consistent with CaO_x crystals. X-ray tomography slice images (acquired along the top-view axis) obtained for a group of CaO_x particle clusters in sample U-1 T (Fig. S1), exposed their hollow morphology resulting from their organized assembly within idioblasts.

SEM image (Fig. 3a) collected for bCuS show particles with sizes of 1–10 μm. Fig. 3b shows the distribution of bCuS on a tomato leaf after dipping treatment. A low population density of small bCuS particles (1–3 μm size range) was observed on the leaf surface, likely due to the rapid sedimentation of larger particles in the suspension during the dipping treatment. Two months after the initial bCuS treatment (bCuS-1 T), X-ray tomography (Fig. S2a) and SEM/EDX analysis (Fig. S2b) reveal the persistence of localized CaO_x crystal pockets within the leaf mesophyll, similar to those observed in the untreated control (U-1 T). This

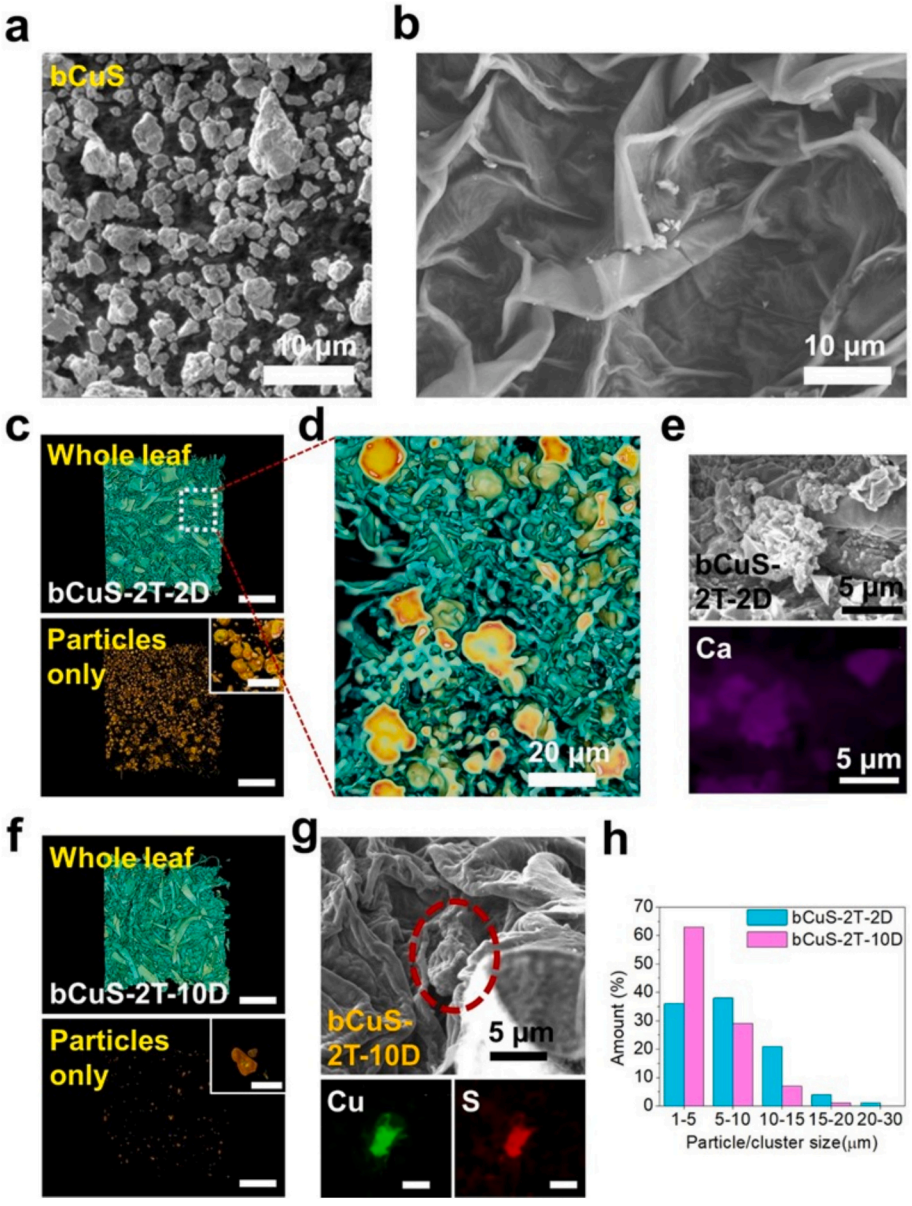

Fig. 3. SEM images of a) bCuS MPs and b) leaf surface after dipping treatment in a 200 mg L^{-1} suspension of bCuS. c) X-ray tomography top view images of sample bCuS-2t-2d showing whole leaf (top) and particles only (bottom). The scale bar is 100 μm. Inset in the particles only top view shows clusters of particle aggregates. The scale bar is 18 μm. d) Slice X-ray tomography image of a segment of bCuS-2t-2d acquired along the top-view axis of image showing whole leaf (dotted square in 3c). e) SEM image and EDX mapping for Ca of particle cluster in sample bCuS-2T-2D. f) X-ray tomography top view images of sample bCuS-2t-10d showing whole leaf (top) and particles only (bottom). The scale bar is 100 μm. Inset in the particles only top view shows clusters of particle aggregates. The scale bar is 18 μm. g) SEM image and EDX mapping for Cu and S of particle cluster in sample bCuS-2T-10D. The scale bar of EDX mapping is 5 μm. h) Particle size distributions of particle clusters from particles only X-ray tomography top view images for bCuS-2T-2D and bCuS-2T-10D.

outcome is expected, as the applied bCuS particles would have largely dissolved or translocated to other tissues by this time, and new leaf growth would have occurred. Notably, significant morphological changes are evident in samples after the second particle sample application. For bCuS-2 T-2D (Fig. 3c and inset), X-ray tomography reveals large, compacted aggregates of particles. Slice X-ray tomography of a leaf segment from bCuS-2 T-2D (Fig. 3d), acquired along the top-view axis, exposes distinct colour contrasts (yellow *vs.* dark orange) within the particles. These core–double-shelled structures are comprised of a composite of high atomic number middle shell and lower atomic number core and outer shell regions. For comparison, X-ray tomography slices of a leaf segment from sample U-1 T (Fig. S3) were analysed to visualize the internal structure of the CaO_x particle clusters. Unlike sample bCuS-2 T-2D, the slices did not exhibit distinct colour contrasts within the clusters, indicating the presence of a single element type. SEM and EDX cross-sectional surveys of bCuS-2T-2D (Fig. 3e) identified large micro-aggregates (~7 μm in size) composed of prismatic and irregular Ca-rich particles, yet no detectable CuS particles or corresponding Cu/S elemental signals were observed. Hence, Figs. 3(c–e) and S3 indicate that the CuS MPs in bCuS-2 t-2d are likely embedded within the aggregates, predominantly occupying the middle shell. In the X-ray tomography image for bCuS-2 T-10D (Fig. 3f and inset), the aggregates appear smaller but denser (darker colour). Here, SEM and EDX analyses of bCuS-2 T-10D (Fig. 3g) confirm the presence of discrete microsized CuS particles (~8 μm) embedded within the leaf tissue, consistent with the particle size distribution observed in the corresponding X-ray tomography images (Fig. 3h). These embedded particles were notably larger than the bCuS particles detected on the leaf surface; in addition, the particle sizes are much larger in bCuS-2 T-2D relative to bCuS-2 T-10D (Fig. 3h).

Next, the interactions of nanoengineered nFeCuS particles were investigated inside the tomato plant leaf. nFeCuS has hollow nanocube morphology of ~500 nm (SEM image in Fig. 4a). Fig. 4b shows the distribution of nFeCuS on a tomato leaf after dip treatment. Contrary to bCuS, a high density of well dispersed nFeCuS NPs was observed on the leaf surface. X-ray tomography imaging (Fig. S4a) and SEM/EDX analysis (Fig. S4b) of the nFeCuS-1 T sample reveal the presence of discrete particle compartments consistent with CaO_x crystals localized within idioblast cells. Compared to bCuS-1 T, these idioblast regions in nFeCuS-1 T appear more densely populated with CaO_x structures. In contrast to the distinct structural transitions evident with leaf samples treated with bCuS, the X-ray tomography and SEM/EDX analyses of the leaf samples after the second nFeCuS NPs application only show slight changes post-treatment (Fig. 4(c–f)). Particle clusters are evident in the X-ray tomography images for sample nFeCuS-2T-2d and nFeCuS-2T-10d (Fig. 4c and e), similar to those found in sample U-1T. SEM leaf cross-sectional imaging of nFeCuS-2T-2D and nFeCuS-2T-10d reveal groups of NPs, which were confirmed by EDX as nFeCuS NP clusters (Fig. 4d and f). The nFeCuS NP clusters were found in close proximity to plant cell boundaries (indicated by orange arrows in Fig. 4d and f), indicative of potentially enhanced bioavailability. Additionally, nFeCuS NPs were observed adhering to the surface of CaO_x crystal aggregates (Fig. S5) without any overt direct physicochemical interaction. Stomatal uptake is indicated as the size and shape of the nFeCuS NPs are maintained in the internal leaf tissues.

STEM coupled with EDX analysis was conducted on ultramicrotomed leaf sections from U-1T, bCuS-1T, and nFeCuS-1T samples. High-angle annular dark field (HAADF) images and corresponding elemental maps for C, O, and Cu are presented in Fig. 5a. The nanoscale globular structures observed, ranging from ~200 to 500 nm in diameter, are likely extracellular vesicles (EVs) [27,28]. EVs are secreted by plant cells and, although their precise biological roles remain ambiguous, they have been implicated in intercellular communication pathways involving the transport of proteins, lipids, and RNAs [27,28]. Many studies have suggested that EVs are opening new frontiers for modern drug delivery [29]. A comparative analysis of Cu distribution discloses an increased Cu content in the EV-like structures in both bCuS-1 T and nFeCuS-1 T samples relative to the untreated control (U-1 T), with the nFeCuS-1 T sample exhibiting a markedly higher Cu signal (Fig. 5b). These findings suggest active or passive incorporation of Cu into plant-derived vesicular compartments.

2.2. Proposed particle-leaf interactions

The biological role of CaO_x crystals remains partially speculative, however, they are widely recognized for their capacity to sequester toxic metal ions (*e.g.*, Al^{3+}, Cd^{2+}, Pb^{2+}, Sr^{2+}, Mn^{2+}) absorbed *via* the root system [19,21,30,31]. Based on the current findings, we propose an analogous protective mechanism for particles, wherein CaO_x crystals mediate the sequestration of foreign particulate matter in the bCuS treated sample upon penetration of the leaf mesophyll space *via* the stomata. A schematic representation summarising the interactions between CuS-based particles and CaO_x crystals is provided in Fig. 5c. Specifically, two days after the second dipping treatment (bCuS-2T-2D), the small bCuS MPs (1–3 μm in size) become encapsulated through a dissolution–recrystallization mechanism mediated by the CaO_x crystals, leading to the formation of large core–double-shell microparticle structures with the bCuS small MPs forming the middle shell. This mechanism likely accounts for the absence of CuS EDX signals in bCuS-2 T-2D, as the particles are fully shielded. CaO_x crystal dissolution and recrystallization at different physiological conditions was demonstrated in *Lemna minor* L. [32]. Also, previous studies have reported CaO_x dissolution and Ca remobilization in plants under specific stress conditions [33–35]. The ability of plants to dissolve and reprecipitate exogenous metal NPs has also been reported [9]. The zeta potential of the particles was measured to estimate their surface charges. The zeta potentials of bCuS and nFeCuS were -15.8 ± 2.3 mV and $+13.18 \pm 0.4$ mV, respectively. The negative zeta potential of bCuS is associated with a higher surface density of sulfide (S^{2-}/S_x^{2-}) species. This negatively charged surface can promote the local accumulation of Ca^{2+} ions present in the mesophyll apoplast, which can react with available oxalate to nucleate CaO_x at the particle interface. The Ca^{2+} and oxalate ions are plausibly supplied through the partial dissolution and remobilization of endogenous CaO_x crystals within idioblast cells, consistent with a dissolution–recrystallization mechanism. Within the confined and heterogeneous mesophyll environment, CaO_x-mediated sequestration is most likely governed by particle size, surface functionalization, and the ability of bCuS to act as heterogeneous nucleation substrate, rather than by classical electrostatic interactions alone. Over time, the sequestered small bCuS MPs coalesced into larger particles and the CaO_x core and shell may dissociate, releasing the aggregated CuS MPs, leading to relocation to extracellular spaces (bCuS-2 T-10D) at distance from metabolically active cells, thereby reducing bioavailability.

Importantly, the presence of citrate molecules and Fe atoms on the surface of nFeCuS NPs may inhibit CaO_x crystallization [36–38]. The positive zeta potential measured for nFeCuS is indicative of a higher surface density of Cu and Fe cations, reflecting distinct surface chemistry compared with bCuS. As a result, electrostatic attraction of Ca^{2+} ions to the nanoparticle surface would be unfavourable, thereby suppressing heterogeneous nucleation of CaO_x at the particle interface. Thus, nFeCuS NPs were not sequestered by CaO_x crystals in either the nFeCuS-2T-2D or nFeCuS-2T-10D samples. Thus, nFeCuS NPs remained dispersed within the mesophyll intercellular spaces, thereby retaining their bioavailability to surrounding plant cells. Upon penetration within leaf tissue, CuS particles undergo partial dissolution and diffusion into plant cells, triggering the formation of EVs enriched in Cu, with the highest concentrations observed in nFeCuS-treated samples. The released Cu species, either as free ions or coordinated in proteins and enzymes, can then be mobilized to distal sites within the leaf or systemically across the plant, potentially reaching pathogen-affected regions as part of a coordinated defence response. Indeed, our previous work showed that Cu-dependent enzymes involved in amine metabolism and ROS-mediated

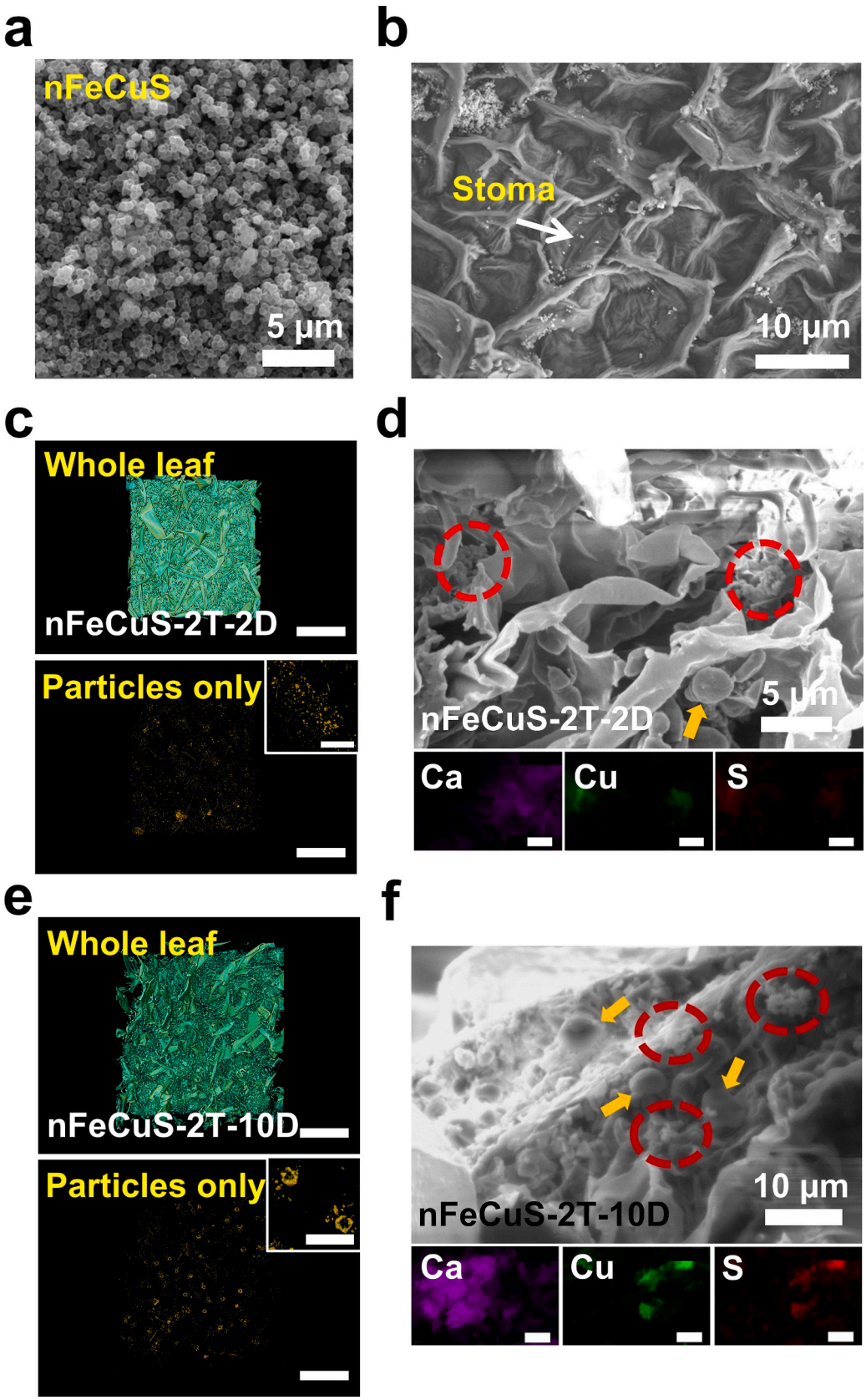

Fig. 4. SEM images of a) nFeCuS NPs and b) leaf surface after dipping treatment in a 200 mg L^{-1} suspension of nFeCuS NPs, with a stoma shown. c) X-ray tomography top view images of sample nFeCuS-2t-2d showing whole leaf (top) and particles only (bottom). The scale bar is 100 µm. Inset in the particles only top view shows clusters of particles. The scale bar is 20 µm. d) SEM image and EDX mapping for Ca, Cu and S in sample nFeCuS-2T-2D. Orange arrows in the SEM image point towards leaf mesophyll cells. The scale bar of EDX mapping is 5 µm. e) X-ray tomography top view images of sample nFeCuS-2t-10d showing whole leaf (top) and

particles only (bottom). The scale bar is 100 μm. Inset in the particles only top view shows clusters of particles. The scale bar is 20 μm. f) SEM image and EDX mapping for Ca, Cu and S in sample nFeCuS-2T-10D. Orange arrows in the SEM image point towards leaf mesophyll cells. The scale bar of EDX mapping is 5 μm.

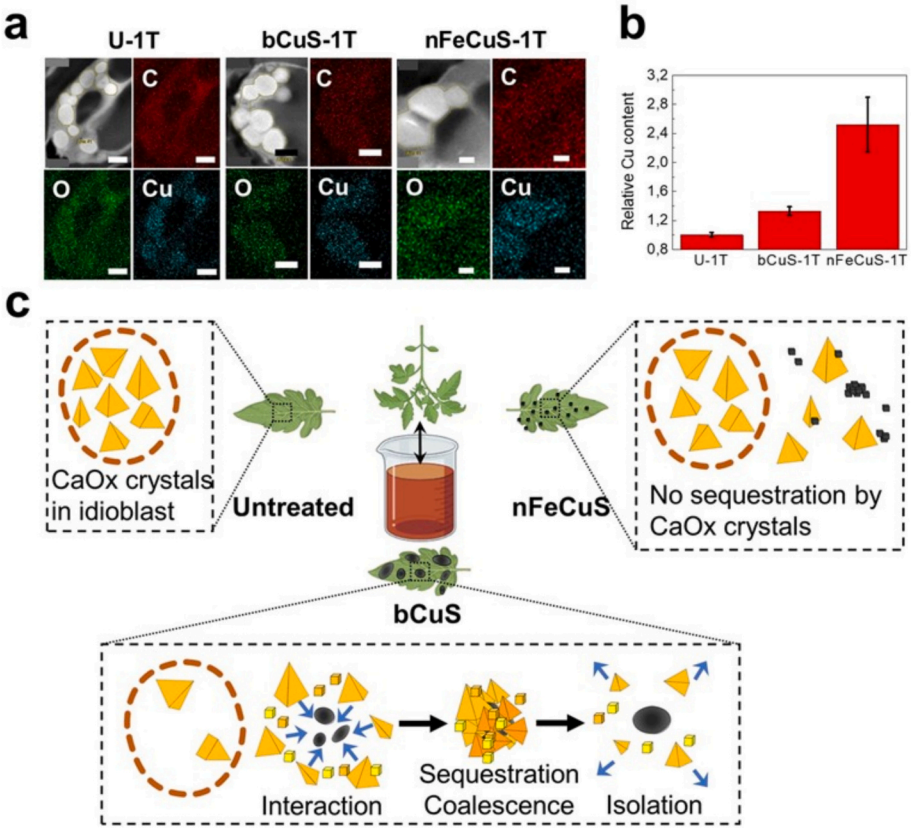

Fig. 5. a) HAADF and C, O and Cu elemental mapping of cell-like structures in U-1T, bCuS-1T and nFeCuS-1T. Scale bars for U-1T and bCuS-1T are 500 nm. Scale bar for nFeCuS-1T is 200 nm. b) Relative Cu content in U-1T, bCuS-1T and nFeCuS-1T. c) Schematic to explain the interaction between CaO_x crystals and CuS particles in tomato leaves.

defence signalling were significantly upregulated in tomato plants treated with nFeCuS NPs, considerably suppressing *Fusarium* wilt disease and enhancing plants growth relative to bCuS treatment [22].

The Ca contents measured by ICP-OES in untreated, nFeCuS-, and bCuS-treated diseased shoot samples were 33,811 ± 3329, 35,505 ± 4119, and 31,262 ± 3078 mg kg^{-1}, respectively, and no statistically significant differences were observed among the treatments (*t*-test, $p > 0.05$). This suggests that calcium uptake by the leaf tissue was not adversely affected by particle treatment. Instead, the observed CaO_x-mediated sequestration appears to involve local redistribution of Ca^{2+} already present within the leaf, rather than altered bulk calcium absorption.

This work focused on state-of-the-art imaging techniques to probe the internal architecture of tomato leaves with and without particle treatments. Building on these findings, future studies will be directed towards further testing the proposed sequestration and evasion mechanisms. Planned efforts include the extraction of CaO_x crystals from tomato leaves, followed by detailed physicochemical characterization of CaO_x, nFeCuS, and bCuS particle surfaces. Laboratory-scale CaO_x crystallization experiments under plant-relevant physiological conditions will be conducted to assess particle-mediated effects on nucleation and growth [39]. Gene expression analyses will be performed to quantify transcriptional changes in pathways associated with oxalate biosynthesis, CaO_x crystal formation and degradation, Ca^{2+} transport, and stress perception and defence [40]. Enzymes and other phytochemicals implicated in CaO_x precipitation and dissolution will be evaluated in untreated leaves and in leaves treated with nFeCuS and bCuS [41].

3. Conclusion

This work provides important preliminary insights into the elegant and intricate molecular interactions underlying observed plant defence and pathology. Fascinatingly, the action of CaO_x crystals on bCuS MPs resembles the engulfing of pathogens by white blood cells in humans, highlighting striking parallels between plant and animal defence systems. We propose that the specific and unique physicochemical properties of nFeCuS, including morphology, nanoscale size, and surface properties, enable them to elude early-stage sequestration and immobilization by CaO_x crystals, that appear to act as a primary plant defence mechanism against metal toxicity. These findings support the use of advanced imaging techniques for the rational design and nano-engineering of next-generation nanovaccines tailored for efficient bioavailability and plant defence activation, enabling significant progress in the deployment of sustainable nano-enabled agriculture to enhance productivity in a rapidly changing climate.

CRediT authorship contribution statement

Yash Boyjoo: Writing – original draft, Visualization, Validation, Software, Methodology, Investigation, Formal analysis, Data curation, Conceptualization. **Junseo Lee:** Writing – review & editing, Software, Methodology, Investigation, Formal analysis, Conceptualization. **Chu-Yun Hwang:** Investigation. **Luyao Qin:** Investigation. **Yi Wang:** Formal analysis. **Jason C. White:** Writing – review & editing. **Qian Chen:** Writing – review & editing, Resources, Funding acquisition. **Archana**

Bhaw-Luximon: Writing – review & editing, Project administration, Funding acquisition.

Declaration of competing interest

The authors declare no competing interests.

Acknowledgements

We would like to thank the Microscopy Suite at the Beckman Institute for Advanced Science and Technology and The Electron Microscopy Suite at The Materials Research Laboratory, Grainger College of Engineering, University of Illinois Urbana-Champaign (USA). Dr. Boyjoo is grateful to Prof Qian Chen's group from the Materials Research Laboratory (MRL) at University of Illinois Urbana-Champaign for hosting him during his research COMPASS CERA Fellowship. This work is funded by the Centre for Complex Particle Systems-Collaboration and Exchange with Researchers in Africa-National Science Foundation (COMPASS-CERA-NSF) program and by the Higher Education Commission (Mauritius) under project vote CBBR T740.

Appendix A. Supplementary data

Supplementary data to this article can be found online at https://doi.org/10.1016/j.cej.2026.173295.

Data availability

Data will be made available on request.

References

[1] N. Mamidi, F. Franco De Silva, A. Orash Mahmoudsalehi, Advanced disease therapeutics using engineered living drug delivery systems, Nanoscale 17 (2025) 7673–7696, https://doi.org/10.1039/D4NR05298F.
[2] S. Shetty, P.C. Alvarado, D. Pettie, J.H. Collier, Next-generation vaccine development with nanomaterials: recent advances, possibilities, and challenges, Annu. Rev. Biomed. Eng. 26 (2024) 273–306, https://doi.org/10.1146/annurev-bioeng-110122-124359.
[3] F. Hameedat, B.B. Mendes, J. Conniot, L.D. Di Filippo, M. Chorilli, A. Schroeder, J. Conde, F. Sousa, Engineering nanomaterials for glioblastoma nanovaccination, Nat. Rev. Mater. 9 (2024) 628–642, https://doi.org/10.1038/s41578-024-00684-z.
[4] D. Bekah, Y. Boyjoo, R. Mistry Panpadoo, J.C. White, A. Bhaw-Luximon, Nanostimulants and nanofertilizers for precision agriculture: transforming food production in the 21st century, Environ. Sci. Nano 12 (2025) 1740–1766, https://doi.org/10.1039/D5EN00055F.
[5] B.N. Kunkel, D.M. Brooks, Cross talk between signaling pathways in pathogen defense, Curr. Opin. Plant Biol. 5 (2002) 325–331, https://doi.org/10.1016/S1369-5266(02)00275-3.
[6] P.V.L. Reddy, J.A. Hernandez-Viezcas, J.R. Peralta-Videa, J.L. Gardea-Torresdey, Lessons learned: are engineered nanomaterials toxic to terrestrial plants? Sci. Total Environ. 568 (2016) 470–479, https://doi.org/10.1016/j.scitotenv.2016.06.042.
[7] P. Faseela, J.M. Joel, R. Johnson, E. Janeeshma, P.P. Sameena, A. Sen, J.T. Puthur, Paradoxical effects of nanomaterials on plants: Phytohormonal perspective exposes hidden risks amidst potential benefits, Plant Physiol. Biochem. 210 (2024) 108603, https://doi.org/10.1016/j.plaphy.2024.108603.
[8] P. Hu, J. An, M.M. Faulkner, H. Wu, Z. Li, X. Tian, J.P. Giraldo, Nanoparticle charge and size control foliar delivery efficiency to plant cells and organelles, ACS Nano 14 (2020) 7970–7986, https://doi.org/10.1021/acsnano.9b09178.
[9] L. Wei, J. Liu, G. Jiang, Nanoparticle-specific transformations dictate nanoparticle effects associated with plants and implications for nanotechnology use in agriculture, Nat. Commun. 15 (2024) 7389, https://doi.org/10.1038/s41467-024-51741-8.
[10] D.V. Francis, A.K. Abdalla, W. Mahakham, A.K. Sarmah, Z.F.R. Ahmed, Interaction of plants and metal nanoparticles: exploring its molecular mechanisms for sustainable agriculture and crop improvement, Environ. Int. 190 (2024) 108859, https://doi.org/10.1016/j.envint.2024.108859.
[11] R. Li, R. Zhang, Y. Li, C. Liu, P. Wang, H. Sun, L. Wang, Foliar uptake and distribution of metallic oxide nanoparticles in maize (*Zea mays* L.) leaf, Environ. Sci. Technol. (2024) acs.est.4c00991, https://doi.org/10.1021/acs.est.4c00991.
[12] J. Lv, P. Christie, S. Zhang, Uptake, translocation, and transformation of metal-based nanoparticles in plants: recent advances and methodological challenges, Environ. Sci. Nano 6 (2019) 41–59, https://doi.org/10.1039/C8EN00645H.
[13] Y. Tang, R. He, J. Zhao, G. Nie, L. Xu, B. Xing, Oxidative stress-induced toxicity of CuO nanoparticles and related toxicogenomic responses in Arabidopsis thaliana, Environ. Pollut. 212 (2016) 605–614, https://doi.org/10.1016/j.envpol.2016.03.019.
[14] G. Feigl, The impact of copper oxide nanoparticles on plant growth: a comprehensive review, J. Plant Interact. 18 (2023) 2243098, https://doi.org/10.1080/17429145.2023.2243098.
[15] H. Shang, C. Ma, C. Li, J.C. White, T. Polubesova, B. Chefetz, B. Xing, Copper sulfide nanoparticles suppress *Gibberella fujikuroi* infection in rice (*Oryza sativa* L.) by multiple mechanisms: contact-mortality, nutritional modulation and phytohormone regulation, Environ. Sci. Nano 7 (2020) 2632–2643, https://doi.org/10.1039/D0EN00535E.
[16] L. Zhao, T. Bai, H. Wei, J.L. Gardea-Torresdey, A. Keller, J.C. White, Nanobiotechnology-based strategies for enhanced crop stress resilience, Nat. Food 3 (2022) 829–836, https://doi.org/10.1038/s43016-022-00596-7.
[17] Y. Wang, C. Deng, W.H. Elmer, C.O. Dimkpa, S. Sharma, G. Navarro, Z. Wang, J. LaReau, B.T. Steven, Z. Wang, L. Zhao, C. Li, O.P. Dhankher, J.L. Gardea-Torresdey, B. Xing, J.C. White, Therapeutic delivery of nanoscale sulfur to suppress disease in tomatoes: in vitro imaging and orthogonal mechanistic investigation, ACS Nano 16 (2022) 11204–11217, https://doi.org/10.1021/acsnano.2c04073.
[18] Y. Wang, C. Deng, L. Zhao, C.O. Dimkpa, W.H. Elmer, B. Wang, S. Sharma, Z. Wang, O.P. Dhankher, B. Xing, J.C. White, Time-dependent and coating modulation of tomato response upon sulfur nanoparticle internalization and assimilation: an orthogonal mechanistic investigation, ACS Nano 18 (2024) 11813–11827, https://doi.org/10.1021/acsnano.4c00512.
[19] V.R. Franceschi, A.M. Schueren, Incorporation of strontium into plant calcium oxalate crystals, Protoplasma 130 (1986) 199–205, https://doi.org/10.1007/BF01276601.
[20] N. Bouropoulos, S. Weiner, L. Addadi, Calcium oxalate crystals in tomato and tobacco plants: morphology and in vitro interactions of crystal-associated macromolecules, Chem. A Eur. J. 7 (2001) 1881–1888, https://doi.org/10.1002/1521-3765(20010504)7:9%253C1881::AID-CHEM1881%253E3.0.CO;2-I.
[21] J.F. Ma, S. Hiradate, H. Matsumoto, High aluminum resistance in Buckwheat1, Plant Physiol. 117 (1998) 753–759, https://doi.org/10.1104/pp.117.3.753.
[22] L. Qin, C. Deng, Y. Boyjoo, S. Sharma, H. Ashraf, M. Wang, L. Zhao, C. Sabliov, A. Bhaw-Luximon, C. Dimkpa, Y. Wang, S. Chen, J.C. White, Nano-stimulated immunity: synthesis and functionalization of CuS induce multi-level defense responses against Fusarium in tomato (*Solanum lycopersicum*) (2026). Manuscript ID: Jf-2025-135277. Article In Press.
[23] C. Ma, J. Borgatta, R. De La Torre-Roche, N. Zuverza-Mena, J.C. White, R. J. Hamers, W.H. Elmer, Time-dependent transcriptional response of tomato (*Solanum lycopersicum* L.) to Cu nanoparticle exposure upon infection with *Fusarium oxysporum* f. sp. *lycopersici*, ACS Sustain. Chem. Eng. 7 (2019) 10064–10074, https://doi.org/10.1021/acssuschemeng.9b01433.
[24] C. Ma, J. Borgatta, B.G. Hudson, A.A. Tamijani, R. De La Torre-Roche, N. Zuverza-Mena, Y. Shen, W. Elmer, B. Xing, S.E. Mason, R.J. Hamers, J.C. White, Advanced material modulation of nutritional and phytohormone status alleviates damage from soybean sudden death syndrome, Nat. Nanotechnol. 15 (2020) 1033–1042, https://doi.org/10.1038/s41565-020-00776-1.
[25] J. Borgatta, C. Ma, N. Hudson-Smith, W. Elmer, C.D. Plaza Pérez, R. De La Torre-Roche, N. Zuverza-Mena, C.L. Haynes, J.C. White, R.J. Hamers, Copper based nanomaterials suppress root fungal disease in watermelon (*Citrullus lanatus*): role of particle morphology, composition and dissolution behavior, ACS Sustain. Chem. Eng. 6 (2018) 14847–14856, https://doi.org/10.1021/acssuschemeng.8b03379.
[26] I. Karmous, S. Vaidya, C. Dimkpa, N. Zuverza-Mena, W. Da Silva, K.A. Barroso, J. Milagres, A. Bharadwaj, W. Abdelraheem, J.C. White, W.H. Elmer, Biologically synthesized zinc and copper oxide nanoparticles using *Cannabis sativa* L. enhance soybean (*Glycine max*) defense against fusarium virguliforme, Pestic. Biochem. Physiol. 194 (2023) 105486, https://doi.org/10.1016/j.pestbp.2023.105486.
[27] E. Cocucci, J. Meldolesi, Ectosomes and exosomes: shedding the confusion between extracellular vesicles, Trends Cell Biol. 25 (2015) 364–372, https://doi.org/10.1016/j.tcb.2015.01.004.
[28] J. Meldolesi, Exosomes and ectosomes in intercellular communication, Curr. Biol. 28 (2018) R435–R444, https://doi.org/10.1016/j.cub.2018.01.059.
[29] I.K. Herrmann, M.J.A. Wood, G. Fuhrmann, Extracellular vesicles as a next-generation drug delivery platform, Nat. Nanotechnol. 16 (2021) 748–759, https://doi.org/10.1038/s41565-021-00931-2.
[30] H. Blommaert, H. Castillo-Michel, G. Veronesi, R. Tucoulou, J. Beauchêne, P. Umaharan, E. Smolders, G. Sarret, Ca-oxalate crystals are involved in cadmium storage in a high cd accumulating cultivar of cacao, Environ. Exp. Bot. 221 (2024) 105713, https://doi.org/10.1016/j.envexpbot.2024.105713.
[31] A.M.A. Mazen, O.M.O. El Maghraby, Accumulation of cadmium, lead and strontium, and a role of calcium oxalate in water hyacinth tolerance, Biol. Plant. 39 (1997) 411–417, https://doi.org/10.1023/A:1001174132428.
[32] V.R. Franceschi, Calcium oxalate formation is a rapid and reversible process in Lemna minor L, Protoplasma 148 (1989) 130–137, https://doi.org/10.1007/BF02079332.
[33] G.M. Volk, V.J. Lynch-Holm, T.A. Kostman, L.J. Goss, V.R. Franceschi, The role of druse and raphide calcium oxalate crystals in tissue calcium regulation in *Pistia stratiotes* leaves, Plant Biol. 4 (2002) 34–45, https://doi.org/10.1055/s-2002-20434.
[34] R. Minocha, S. Long, Seasonal changes in foliar calcium oxalate concentrations in conifer and hardwood trees: a potentially bioavailable source of cellular calcium and/or oxalate under stress, Front. For. Global Change 6 (2023) 1161088, https://doi.org/10.3389/ffgc.2023.1161088.
[35] O. Gómez-Espinoza, D. González-Ramírez, P. Bresta, G. Karabourniotis, L.A. Bravo, Decomposition of calcium oxalate crystals in Colobanthus quitensis under CO2

limiting conditions, Plants 9 (2020) 1307, https://doi.org/10.3390/plants9101307.
[36] M.J. Nicar, K. Hill, C.Y.C. Pak, Inhibition by citrate of spontaneous precipitation of calcium oxalate *in vitro*, J. Bone Miner. Res. 2 (1987) 215–220, https://doi.org/10.1002/jbmr.5650020308.
[37] E. Ruiz-Agudo, A. Burgos-Cara, C. Ruiz-Agudo, A. Ibañez-Velasco, H. Cölfen, C. Rodriguez-Navarro, A non-classical view on calcium oxalate precipitation and the role of citrate, Nat. Commun. 8 (2017) 768, https://doi.org/10.1038/s41467-017-00756-5.
[38] J.A. Muñoz, M. Valiente, Effects of trace metals on the inhibition of calcium oxalate crystallization, Urol. Res. 33 (2005) 267–272, https://doi.org/10.1007/s00240-005-0468-4.
[39] S. Menon, A.S. Al-Saadi, N.J. Al-Aamri, A.-Z.H. Al-Jaradi, H.K. Al Mamari, L.H. Al Haddabi, V.P. Jayachandran, C.B. Shinisha, Inhibition of crystallization of calcium oxalate monohydrate using leaves from different species of Moringa – experimental and theoretical studies, J. Cryst. Growth 598 (2022) 126859, https://doi.org/10.1016/j.jcrysgro.2022.126859.
[40] M.-I. Khan, N. Bashir, S. Pandith, M. Shah, Z. Reshi, A. Shahzad, Rhubarb: a novel model plant to study the conundrum of calcium oxalate synthesis, Food Chem. 434 (2024) 137458, https://doi.org/10.1016/j.foodchem.2023.137458.
[41] X. Li, D. Zhang, V.J. Lynch-Holm, T.W. Okita, V.R. Franceschi, Isolation of a crystal matrix protein associated with calcium oxalate precipitation in vacuoles of specialized cells, Plant Physiol. 133 (2003) 549–559, https://doi.org/10.1104/pp.103.023556.